Title: Gyro-average method for global gyrokinetic particle simulation in realistic tokamak geometry

Yihao Duan[1], Yong Xiao[1] (*), Zhihong Lin[2]
[1] IFTS, Zhejiang University, Hangzhou, China 310027
[2] Physics & Astronomy, University of California, Irvine, CA, USA 92697
[*] Electronic mail: yxiao@zju.edu.cn

Abstract:

Gyro-average is a crucial operation to capture the essential finite Larmor radius effect (FLR) in gyrokinetic simulation. In order to simulate strongly shaped plasmas, an innovative multi-point average method based on non-orthogonal coordinates has been developed to improve the accuracy of the original multi-point average method in gyrokinetic particle simulation. This new gyro-average method has been implemented in the gyrokinetic toroidal code(GTC). Benchmarks has been carried out to prove the accuracy of this new method. In the limit of concircular tokamak, ion temperature gradient (ITG) instability is accurately recovered for this new method and consistency is achieved. The new gyro-average method is also used to solve gyrokinetic Poisson equation, and its correctness has been confirmed in the long wavelength limit for realistic shaped plasmas. The improved GTC code with the new gyro-average method has been used to investigate the ITG instability with EAST magnetic geometry. The simulation results show that the correction induced by this new method in the linear growth rate is more significant for short wavelength modes where finite Larmor radius (FLR) effect becomes important. Due to its simplicity and accuracy, this new gyro-average method can find broader applications in simulating the shaped plasmas in realistic tokamaks.

1. Introduction

First-principles gyrokinetic simulation has been widely adopted to study low frequency micro instabilities and turbulences in magnetic fusion plasmas [1,8]. The gyro-average transformation, a frequent operation used in the gyrokinetic simulation, is a procedure to average physical quantities such as electric potential and charge density along the cyclotron orbit[12-14]. To preserve the finite Larmor radius (FLR) effect, the gyro-average needs to be accurate enough to achieve high numerical fidelity. As one of the numerical algorithms for performing gyro-average, the multi-point average method has been developed and used extensively in the gyrokinetic particle simulation[1,3].

Simulations with realistic tokamak geometry, which is usually characterized by features such as up-down asymmetry and non-circularity, is crucial to interpret and predict various complicated tokamak experimental phenomena[10,15,16]. However, such geometric characteristics will lead to a large deviation from regular grid distribution and coordinate orthogonality. These deviations bring significant numerical challenges to the multi-point average method in the gyrokinetic simulation.

In this article, an innovative multi-point method based on non-orthogonal magnetic coordinates has been developed and implemented in the global gyrokinetic toroidal code GTC [8]. This new method modifies the original multi-point average procedure in GTC to accommodate arbitrary magnetic geometry with sufficient concision and high accuracy, and capture more precisely the FLR effect that is important in computing linear eigenmodes and nonlinear turbulence [1]. Due to its simplicity and accuracy, the new method may be implemented to other gyrokinetic codes for simulating experimental plasmas.

Let us detail the physical quantities and equations involving gyro-average in the gyrokinetic particle simulation. Generally, two classes of equations involve this gyro-average procedure, namely the Maxwell's equations to solve for self-consistent electromagnetic fields and equations of motion to push gyrocenters in phase space. To evolve the position and velocity of the gyrocenter, the gyro-averaged magnetic field and electric field is needed in the equations of motion, e.g., the gyro-averaged electrostatic potential $\bar{\phi}$ is defined as

$$\bar{\phi}(\mathbf{R})=\frac{1}{2\pi}\int\phi(\mathbf{x})\delta(\mathbf{x}-\mathbf{R}-\boldsymbol{\rho})d\mathbf{x}d\varphi \tag{1}$$

where $\mathbf{R}$ is the gyrocenter position, $\mathbf{x}$ is the particle position, and φ stands for the gyrophase angle. The Larmor radius $\boldsymbol{\rho} \equiv -\mathbf{v}_\perp \times \hat{b} / \Omega$ with $\hat{b} \equiv \mathbf{B}/B$ and $\Omega \equiv qB/mc$. In the electrostatic limit, the Maxwell's equations can be simplified to be the gyrokinetic Poisson equation, which is essentially the quasi-neutrality condition with the validity limit of $k^2\lambda_d \le 1$:

$$\frac{\tau}{\lambda_d^2}(\phi - \tilde{\phi}) = 4\pi e(\delta\overline{n}_i - \delta n_e) , \tag{2}$$

where $\tau \equiv T_e / T_i$, $\lambda_d \equiv \sqrt{T_e / 4\pi n_0 e^2}$ is the electron Debye length, n_0 is the equilibrium particle density, and the electrostatic potential ϕ is the unknown to be solved for. In Eq. (2), $\delta\overline{n}_i$ and δn_e are the gyro-averaged ion and electron density, respectively, with $\delta\overline{n}_\iota$ defined as

$$\delta\overline{n}_i = \frac{1}{2\pi n_0}\int \delta f_i(\mathbf{R},\mu,v_\parallel)\delta(\mathbf{R}-\mathbf{x}+\boldsymbol{\rho})d\mathbf{R}d\mu dv_\parallel d\varphi , \tag{3}$$

where μ is the magnetic moment, $v_\parallel$ is the parallel velocity, and δf_i is the perturbed ion gyrocenter distribution. In Eq. (2), $\tilde{\phi}$ is the second gyro-averaged potential or double gyro-averaged potential, and it is defined as

$$\tilde{\phi}(\mathbf{x}) = \frac{1}{2\pi}\int \overline{\phi}(\mathbf{R})F_M(\mathbf{R},\mu,v_\parallel)\delta(\mathbf{R}-\mathbf{x}+\boldsymbol{\rho})d\mathbf{R}d\mu dv_\parallel d\varphi \tag{4}$$

where F_M is the Maxwellian distribution of the gyrocenter, And the gyro-averaged electric potential $\overline{\phi}(\mathbf{R})$ can be calculated by Eq. (1).

As is discussed, the gyro-average transformation needs be performed on the electromagnetic fields and charge density to push gyrocenters in the phase space, and the second gyro-average transformation needs to be performed on the electrostatic potential to solve for the electromagnetic fields via the Poisson equation. Such gyro-averaged quantities can be calculated in the wave number ($\mathbf{k}$) space. However, the spectral method is mostly conveniently implemented in the flux-tube simulations, which drops off the background profile effects and is essentially a local approximation[3]. The multi-point average method (typically four-point) has been developed to evaluate the gyro-averaged quantities numerically, which is usually more advantageous in real space for global simulations [1,3]. For the second gyro-average, there is another approach based on the Pade approximation [9], i.e., evaluating the second gyro-averaged potential $\tilde{\phi}$ by $\tilde{\phi} = \phi/(1-\rho_i^2\nabla_\perp^2)$. The Pade approximation can change the double integral operation of $\tilde{\phi}$ to be a second-order differential form and thus avoid the complicated multi-point average procedure, which can be used to solve the gyrokinetic Poisson equation for strongly shaped plasmas [10].

In practice, the multi-point average method could be more accurate than the Pade approximation for short wavelength modes with $k^2\rho_i^2 \geq 1$[3]. However, the original multi-point method implemented in the GTC code is designed for orthogonal or weakly non-orthogonal coordinate systems [3]. It remains a bottleneck for the multi-point average method to accurately simulate strongly shaped plasmas.

In this paper, we present an innovative multi-point average method based on non-orthogonal magnetic coordinates, which can simulate arbitrary shaped plasmas. This new method is implemented in the GTC code and then carefully benchmarked. The GTC simulation results show that the correction induced by this new method does make a difference on the ITG growth rates for the short wavelength modes where the finite Larmor radius (FLR) effect becomes important. The remainder of this paper is organized as follows. The necessity of finding a new gyro-average method for strongly shaped plasma has been introduced in Section 2. The scheme for new multi-point gyro-average method is illustrated in Section 3. Then we present two examples to benchmark this new gyro-average method in Section 4. The new gyro-average method has been applied to study the ITG modes in Sec.5. Section 6 summarizes this paper and discusses the possible future work.

2. Original four-point average method

In this section, we review the original four-point average method based on the magnetic coordinates that is implemented in the GTC code.

The magnetic flux coordinates have been widely used for describing the equilibrium magnetic field of toroidal confinement systems [5] in the gyrokinetic simulations. A particular set of magnetic flux coordinates, namely the Boozer coordinates [6] (ψ,θ,ζ), is chosen in the GTC code to push particles and solve for electromagnetic fields, where ψ is the poloidal flux or radial like variable, θ is the poloidal angle, and ζ is the toroidal angle. With the Boozer coordinates, we can conveniently define a field-aligned mesh which captures the essential flute mode structure of turbulence with $k_{\|} \ll k_{\perp}$, and requires only a few dozens of toroidal grids to accelerate field calculation by a factor varying from several tens to hundreds [10].

The next two approximations have been employed in GTC code without losing accuracy and facilitates the numerical implementation of the four-point average procedure for large aspect ratio tokamaks. First, the toroidal angle in the Boozer coordinates ζ is approximated to the toroidal angle in the cylindrical coordinates (R,ϕ_t,Z) with $\zeta \approx -\phi_t$, Since the difference function $\nu(\psi,\theta) \equiv \zeta + \phi_t$ turns out to be of order $O\left(\varepsilon^2\right)$ for tokamaks with the inverse aspect ratio $\varepsilon = r/R_0 \ll 1$. Second, the perpendicular plane is approximated to the poloidal plane, since the intersection angle δ between them is second order small in ε, i.e. $\delta \sim \mathrm{O}\left(\varepsilon^2/q^2\right)$, which comes from evaluating $\cos\delta = \mathbf{B}\cdot\nabla\zeta / B\left|\nabla\zeta\right|$. For example, it is evaluated numerically that the intersection angle δ is no more than 0.089 for the typical EAST equilibrium, as is shown in Section 5

The original four-point average method has been widely used and well benchmarked for weakly shaped plasma [3,10]. However, strong shaping of the magnetic flux could lead to significant deviation against the implicit assumption in the original four-point scheme. Here we illustrate this deviation and necessity for improvement via using a single-null-divertor equilibrium configuration of the EAST tokamak (Shot # 077741.03500). Fig. 1 shows GTC's field mesh setting on the toroidal plane with $\zeta=0$. The GTC code uses evenly spaced radial grids at $\theta=0$, as is shown by the black straight line in Fig.1(b). In the poloidal direction, the grid size $\Delta\theta$ is uniform on each flux surface while maintaining $r\Delta\theta \sim \Delta r$, as is shown in Fig.1(b). The corresponding grid setting on the (ψ,θ) plane is shown in Fig. 1(a). The relatively regular grid distribution on the (ψ,θ) plane offers great convenience for numerical operations such as field interpolation and particle deposition.

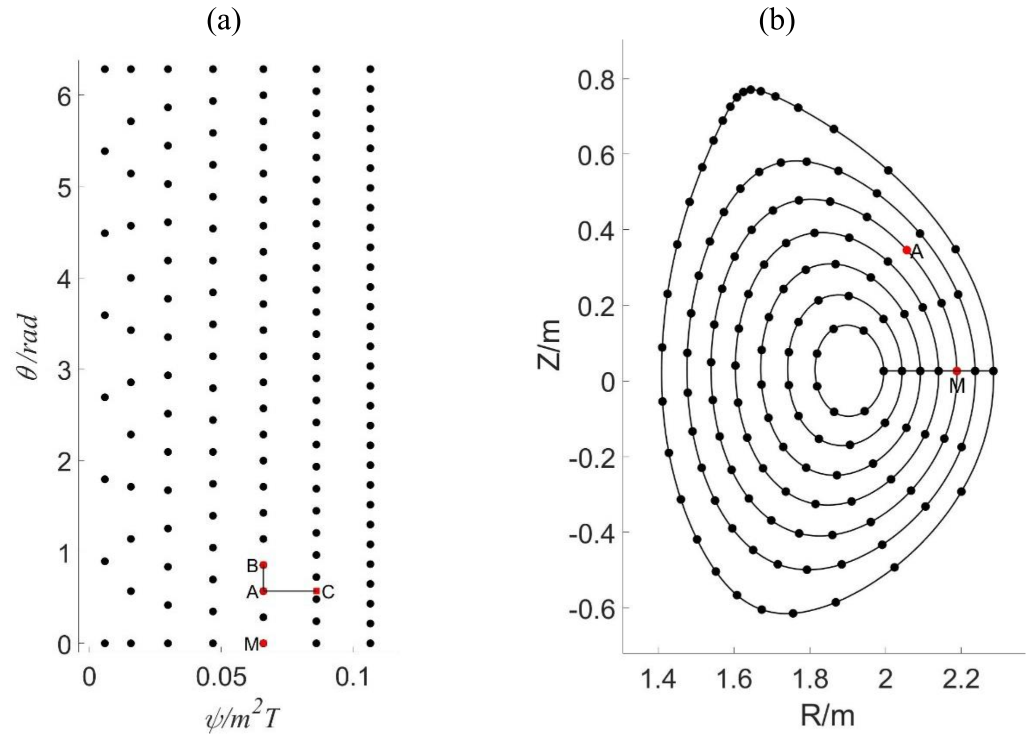

Fig.1 Example of mesh grid distribution on (a) the (ψ,θ) plane and (b) the (R,Z) plane for a typical EAST shaped plasmas (Shot # 077741.03500).

To illustrate the original four-point average method, we consider one particular field point A with the coordinates (ψ,θ) in Fig.1 as the gyrocenter position for gyro-average. In Fig. 1(a), Point B is the poloidal grid next to the field point A along constant ψ, and Point C is the intersection point on the next flux surface along constant θ. In the original method, the four points selected for gyro-average are located at $(\psi \pm \delta\psi, \theta)$ and $(\psi, \theta \pm \delta\theta)$, which are supposed to center at (ψ,θ) with a radius ρ_i. The difference $\delta\psi$ and $\delta\theta$ are calculated by the following relationship:

$$\delta\psi = \frac{\rho_i}{l_{AC}}\psi_{AC}\ ,\ \delta\theta = \frac{\rho_i}{l_{AB}}\theta_{AB} \tag{5}$$

where $\psi_{AC} = \psi_C - \psi_A, \theta_{AB} = \theta_B - \theta_A$. Using the constructed B-splines in GTC[10], the (R, Z) coordinates can be calculated for the selected four points. l_{AC} and l_{AB} can be calculated by $\sqrt{(R_A - R_C)^2 + (Z_A - Z_C)^2}$ and $\sqrt{(R_A - R_B)^2 + (Z_A - Z_B)^2}$, respectively.

After calculating $\delta\psi$ and $\delta\theta$, we present the selected four points $(\psi \pm \delta\psi, \theta)$ $(\psi, \theta \pm \delta\theta)$ in Fig.2 by four red square markers. It can be seen that these four squares are close to equally spaced points on the circle centered about the field point M, as is shown in Fig.2(a); but they are far away from equally spaced points on the circle centered about the field position A, as is shown in Fig.2(b). To figure out why this inaccuracy arises, we draw two contour lines with constant ψ and θ, respectively. These two lines intersect at the point M and A respectively, as is shown by Fig.2 (a) & (b). The constant ψ line is almost orthogonal to the constant θ line in Fig. 2(a) while far away from orthogonal in Fig. 2(b). It is the non-orthogonality of the Boozer coordinates (ψ, θ), or the non-orthogonality of $\nabla\psi$ and $\nabla\theta$, that causes the uneven distribution of the selected four points on the gyro-average circle. Actually, we tested various field points in the whole poloidal plane, and we find that the selected four points are much more inaccurate for gyro-average in the plasma edge than that in the plasma core, since the non-orthogonality of the Boozer coordinates are more severe in the plasma edge.

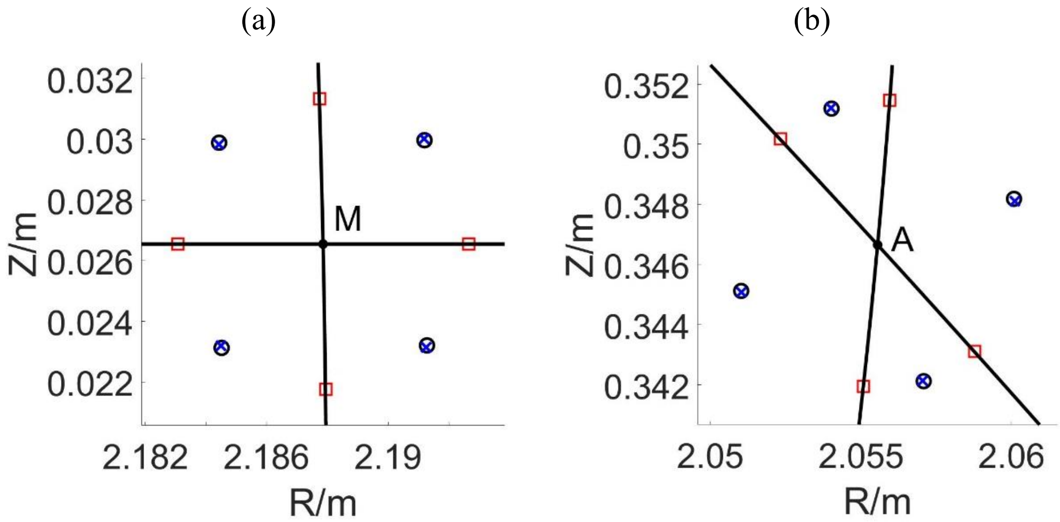

Fig.2 Demonstration of the four point average at the field grid point A: the black circles are the exact points in the four point average method, the red squares are from the original gyro-average method, and the blue crosses are produced by the improved gyro-average method. The two solid lines are the contour lines for constant ψ and θ, respectively.

To quantify how much inaccuracy the original four-point method can bring by the coordinate non-orthogonality, we define α as the intersection angle between $\nabla\psi$ and $\nabla\theta$ ranging from 0 to π and α can be calculated by

$$\cos\alpha = \frac{\nabla\psi \cdot \nabla\theta}{|\nabla\psi||\nabla\theta|} \tag{6}$$

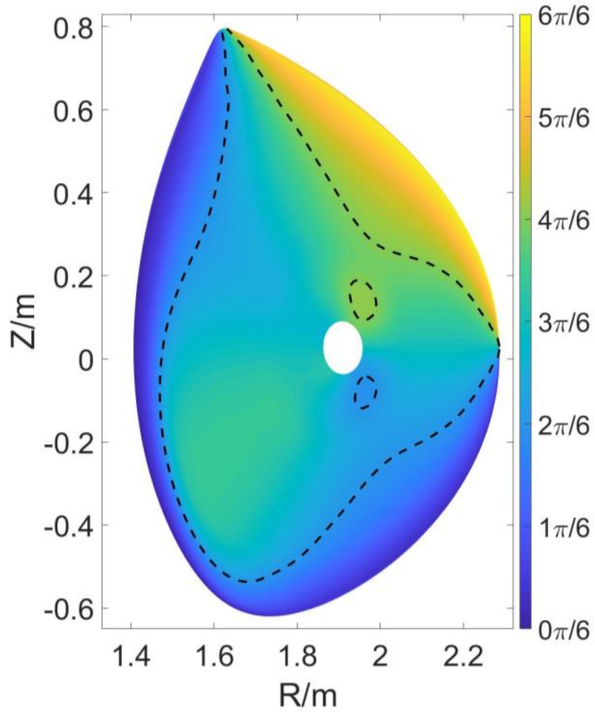

Fig.3 Contour plot for the intersection angle α on the poloidal plane with the contour lines at $\alpha=2\pi/6$ and $\alpha=4\pi/6$ shown by the dashed black lines.

Then we show the intersection angle α in the 2D contour plot of Fig. 3. As can be seen, the angle α is exactly equal to $\pi/2$ at $\theta=0$ where the point M is located. About 45% of the whole area has a moderate angle deviation (less than 30%) from $\pi/2$. The derivation is more severe in those areas close to the plasma edge, as is shown by Fig.3. In some edge areas, the deviation could be even larger than 60%.

3. Improved gyro-average for shaped plasmas

A new numerical method is highly in demand to accommodate this coordinate non-orthogonality for the strongly shaped plasmas. The key idea of this new method is to locate the accurate positions for the gyro-average points by including the non-orthogonality between the radial and poloidal coordinates. The positions of these gyro-average points produced by the new method are given by $(\psi+\Delta\psi_j,\theta+\Delta\theta_j)$ with

$$\Delta\psi_j=\sin(\frac{2\pi j}{N}+\frac{\alpha}{2})\frac{\delta\psi}{\sin(\alpha)},\Delta\theta_j=\sin(\frac{2\pi j}{N}-\frac{\alpha}{2})\frac{\delta\theta}{\sin(\alpha)},(j=1,2,...,N), \quad (7)$$

where the intersection angle α is given in Eq. (6), $\delta\psi$ and $\delta\theta$ are defined by Eq.(5).

N could be 4,8 and et. al., corresponding to the number of points used for the gyro-average. Assuming that $N=8$, the schematic diagram for this new eight-point average method is shown in Fig.4. Two contour lines for constant ψ and θ are shown by the two black solid lines. The vectors $\nabla\psi$ and $\nabla\theta$ are marked in Fig.4, which are perpendicular to their contour lines, respectively. As is shown in Fig.4, the new method produces eight points systematically by $(\psi+\Delta\psi_j, \theta+\Delta\theta_j)$, $j=1,2...8$.

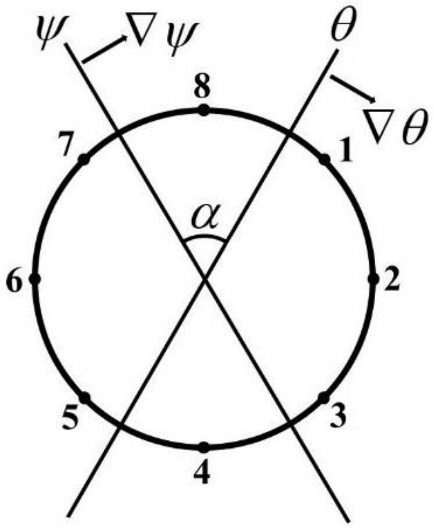

Fig.4 Illustration of the improved gyro-average method based on non-orthogonal coordinates.

The four-point or sixteen-point for average can be produced by the same strategy. For example, we can select four points from the eight points in Fig. 4, namely the points with index j =2,4,6,8, to carry out the four-point average procedure, as is shown in Fig. 2 by the blue crosses. By comparison, we also show the exact points by a brutal force calculation in Fig.2 using black circles. It can be seen that the selected four points from the improved gyro-average method well match the exact four points. To verify the accuracy and generality of new method, we tested various field points in different equilibrium magnetic configurations, such as CFETR (China Fusion Engineering Test Reator). The correction effect of the new method are similar to that presented in Fig.2.

One may argue that the contour lines for constant ψ and θ may not be straight lines within the range of one gyro-orbit and thus numerical inaccuracy could arise.

However, for typical fusion plasmas, the ratio between gyro-radius and the curvature radius of field line is of order $O(\rho_i / R_0)$. Thus, this new method can be used to improve the original gyro-average operation in GTC within satisfactory accuracy. In addition, this improved gyro-average method possesses a number of highly desirable features such as systematic treatment of points and minimal modification to the original GTC code, which make this new method appealing not only to GTC but also to other gyrokinetic codes.

4. Benchmarks for improved gyro-average method

In this section, we implement the improved gyro-average method in the GTC code and verify its effectiveness with two examples. First of all, the improved four-point method should conform with the original four-point average method in the limit of concentric circular tokamak where the original procedure is still accurate. Secondly, it's crucial to verify the accuracy of the improved four-point method by solving the classical Poisson problem $-\nabla_\perp^2 \phi = \delta n$ correctly with realistic geometry.

4.1 Consistency check: Concentric circular geometry

For the concentric circular magnetic field, the magnetic surface is determined by the following equation,

$$R = R_0 + r\cos\theta_g \tag{8}$$

$$Z = r\sin\theta_g \tag{9}$$

The Boozer coordinates (ψ, θ, ζ) are constructed analytically as the following: the poloidal magnetic flux ψ can be determined by $d\psi_t / d\psi = q(\psi)$ with the toroidal magnetic flux $\psi_t = r^2/2$. The Boozer poloidal angle θ can be determined by $\theta = \theta_g - r\sin\theta_g$, and the Boozer toroidal angle ζ can be determined by $\zeta = -\phi_t$. Now we can calculate the intersection angle α in Eq. (6). This angle turns out to be not far away from $\pi/2$, with a deviation of less than 5% in most areas and maximum value of 17% for the large aspect ratio tokamak with $r/R < 0.3$. As we have discussed in

Section 2, the main inaccuracy for the original four-point average method comes from the non-orthogonality between $\nabla\psi$ and $\nabla\theta$. Since the non-orthogonality is weak in this case, the inaccuracy is insignificant according to our analysis. Therefore, the improved four-point average method should conform with the original scheme.

To confirm our conjecture, we use the Cyclone Base parameters in Ref.[7] to carry out a global gyrokinetic simulation via the GTC code for ion temperature gradient (ITG) instability, with the concentric circular geometry defined in Eq. (8) and (9) for the equilibrium magnetic field. The background temperature and density are set as $T_e = T_i = 2.223kev$ and $n_i = n_e = 7.9\times10^{19} m^{-3}$, respectively. The inverse aspect ratio is set as $a/R_0 = 0.36$ with the major radius $R_0 = 0.835\, m$, and the simulation domain is set as $r \subset [0.1a, 0.9a]$. At $r = a/2$ flux surface, we have the following local simulation parameters: $r/R_0 = 0.18$, safety factor $q = 1.4$, magnetic shear $s = q'r/q = 0.78$, density gradient $R_0/L_n = 2.22$, ion or electron temperature gradient $R_0/L_T = 6.92$, where L_T and L_n are the temperature and density gradient scale lengths, defined by $L_T \equiv -(d\ln T/dr)^{-1}$ and $L_n \equiv -(d\ln n/dr)^{-1}$. Here we focus on the ion physics and plasma shaping effect, and the electrons are assumed adiabatic for simplicity.

The linear simulation results on the ITG dispersion are demonstrated in Fig. 5. The linear dispersion relation from this improved gyro-average method matches that from the original gyro-average method in both growth rate and real frequency with a difference less than 5%. Thus, we confirm that the improved gyro-average method is consistent with the original gyro-average method in the limit of concentric circular tokamak, as it should be.

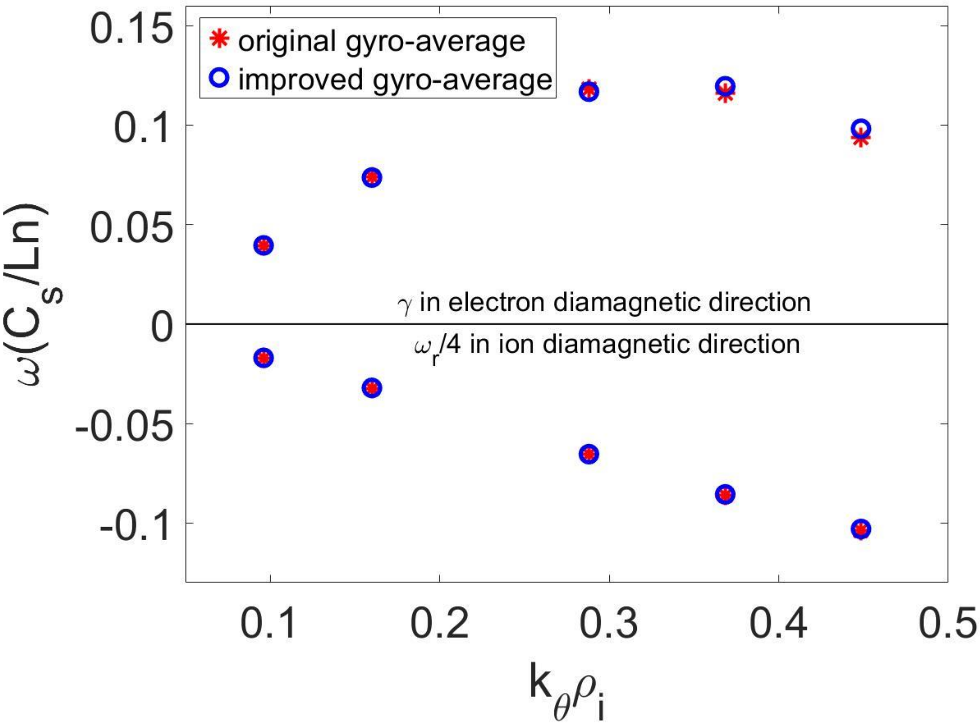

Fig.5 growth rate and real frequency vs wavenumber in concircular geometry.

4.2 Gyrokinetic Poisson solver: EAST magnetic geometry

Next, we come to solve the gyrokinetic Poisson equation Eq.(2) in the long wavelength limit with a typical shaped plasma equilibrium from EAST tokamak experiments. Note that the gyrokinetic Poisson equation becomes two-dimensional in the limit of $k_{\|} \ll k_{\perp}$ and becomes the standard Poisson problem $-\rho_i^2 e n_0 \nabla_\perp^2 \phi = T_i \delta n$ since the approximation $\phi - \tilde{\phi} \approx -\rho_i^2 \nabla_\perp^2 \phi$ holds in the long wavelength limit.

Various benchmarks[3,10] on the four-point average method have been carried out in the large aspect ratio circular cross section limit since the Poisson problem is essentially a Bessel problem in this limit and its solutions are known analytically. However, such experience cannot be easily applied to the realistic shaped geometry where the new method is expected to make a notable difference. A new numerical scheme has been designed to verify the accuracy of the Poisson solver with the improved four-point average by the following procedure : (1) Given a known analytic function expression $F(\psi,\theta)$; (2) calculate the charge density δn numerically by

$\delta n \equiv -\nabla_{\perp}^{2} F$; (3) use the resulting δn as the source to the Poisson equation and solve the Poisson equation $-\nabla_{\perp}^{2}\phi = \delta n$ by employing the four-point average method; (4) Compare the calculated ϕ with the original function $F(\psi,\theta)$ and compute the error by their difference. If $F \approx \phi$ or the error is sufficiently small, we can conclude that this four-point average method is sufficiently accurate.

In this benchmark case, the aforementioned EAST equilibrium is used for the shaped plasma. The specific benchmark function is given by: $F(\psi,\theta) = (\psi - \psi_0)^3(\psi_1 - \psi)^3 \cos(m\theta)$ with $m = 6$, where $\psi_0 = \psi(r = 0.55a)$ and $\psi_1 = \psi(r = 0.95a)$ are the poloidal flux at the inner and outer boundary, respectively.

(a) (b)

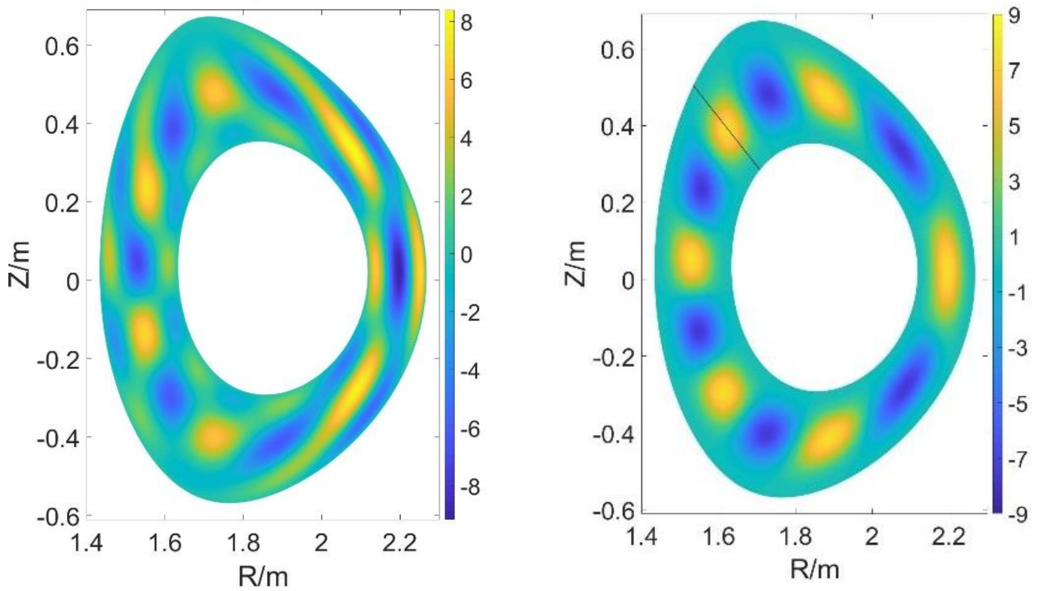

(c) (d)

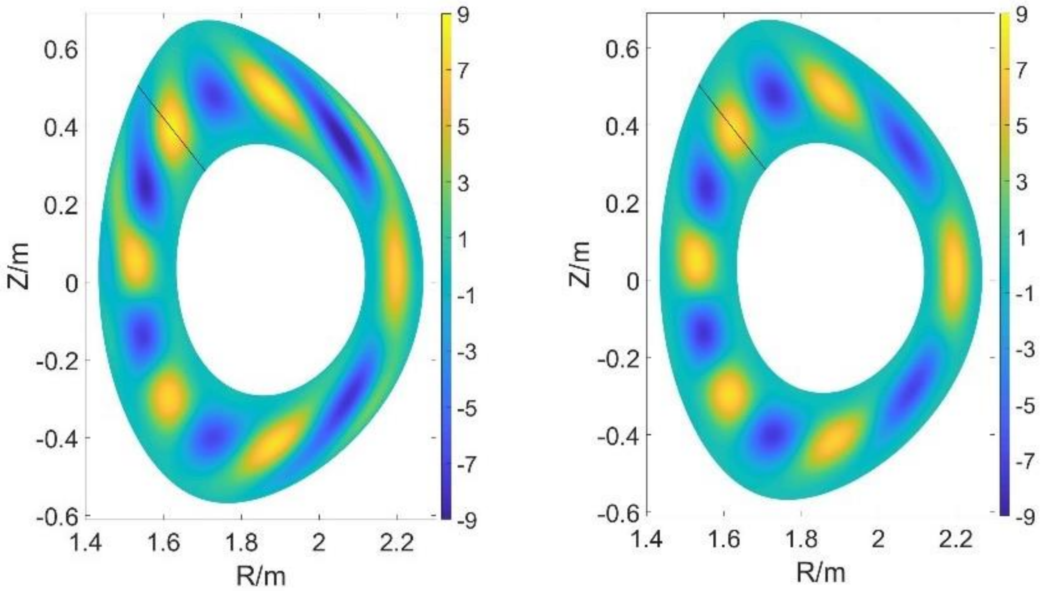

Fig.6 (a) density fluctuation δn on poloidal plane. (b) given analytic function F on poloidal plane. (c) numerical solution ϕ from original four-average method. (d) numerical solution from improved four-average method.

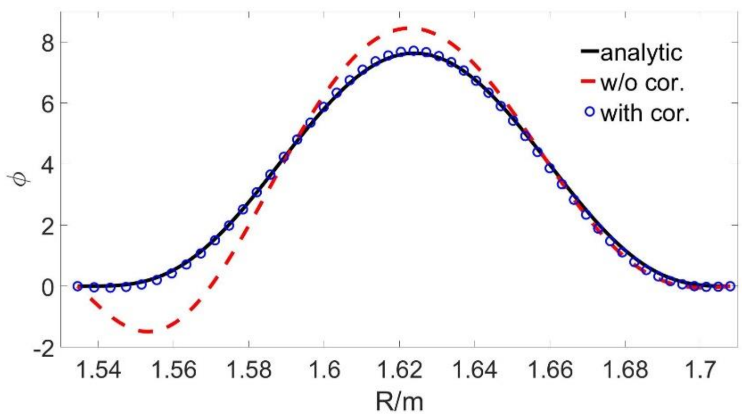

Fig.7 Comparison of solutions along the black line in Fig.6.

The resulting charge density δn is shown in Fig.6 (a). The prescribed function $F(\psi,\theta)$ is shown in Fig. 6 (b), which is also the analytic solution the Poisson equation $-\nabla_{\perp}^{2}\phi=\delta n$. As can be seen, the difference between δn and $F(\psi,\theta)$ is significant. The numerical solution to the Poisson equation is demonstrated in Fig. 7(c) where the original four-point average method is used, and in Fig. 7(d) where the improved four-point average method is used. The numerical solution in Fig.7(d) is almost identical to the analytical solution in Fig.7(b), which proves the accuracy of the improved four-point average method. However, the numerical solution in Fig. 7(c) differs from the analytical solution in Fig.7(b), and its 2D pattern is more like that of the source term δn in Fig. 7(a).

For more quantitative comparison, we take out the data along the black solid line in Fig. 6 (b)(c)(d) and compare them in a one-dimensional plot in Fig.7, where the black line represents the analytical solution F, the blue circle stands for the numerical solution using the improved four-point average method, and the dashed red line represents the numerical solution using the original four-point average method. As can be seen in Fig. 7, there is a notable difference between the red dashed line and the black solid line especially on the left or central side of the figure. We further note that this difference exists not only on this particular line but also on the whole poloidal plane, which suggests that original four-point average needs to be improved for better accuracy. However, the difference is almost indistinguishable between the blue circles and black solid line, which verifies the high accuracy of the improved four-point average method. By scanning the whole poloidal plane, we find that the numerical solution using the improved four-point method matches the exact analytic solution very closely. The slight difference between them comes from the difference of numerical operator. The operator for the four-point average method in this benchmark is $0.7194J_0^2(0.9130k_\perp\rho_i)+0.2806J_0^2(2.2339k_\perp\rho_i)-1$, the exact operator we wanted is $(k_\perp\rho_i)^2$. In the long wavelength limit $k_\perp\rho_i\to 0$, the two operators can be considered as the same. However, there is always a difference between these two operators when $k_\perp\rho_i$ is finite, albeit it is small when $k_\perp\rho_i$ is small.

Combine both benchmarks in this section and the verification in section 3, we conclude that the improved four-point average method can be utilized to significantly improve the gyro-average procedure to obtain an accurate gyro-averaged potential as well as ion density, which is crucial for the PIC simulation to simulate shaped plasmas because the inaccuracy in the gyro-average can accumulate at each time step and may substantially modify the linear and nonlinear simulation results.

5. ITG mode for EAST geometry

In this section, we carry out the ITG simulation with adiabatic electrons using the aforementioned EAST the equilibrium (shot# 077741.03500). The equilibrium data, such as poloidal flux $\psi(R,Z)$, poloidal current I and safety factor q have been used to construct the equibrium magnetic field in real space and determine the Boozer coordinates (ψ,θ,ζ). This shaped EAST equilibrium has an background magnetic field with up-down asymmetry and following tokamak parameters: $B_0 = 2.46T$, $a = 0.375m$, $R_0 = 1.91m$. On the reference flux surface at the middle of the minor radius: $T_i = T_e = 1500ev$ and $n = 4.0\times10^{19} / m^3$. For simplicity, we choose the Cyclone base case parameters $R_0 / L_n = 2.22$, $R_0 / L_T = 6.92$ for the plasma gradients.

The intersection angle between the Boozer coordinates ψ and θ has been computed in Fig.3, and the moderate coordinate non-orthogonality suggests that the improved gyro-average method can play an important role according to the preceding discussions.

The gyro-average procedure is associated with the finite Larmor radius (FLR) effect, an essential kinetic effect in magnetized plasmas. The more accurate we treat the gyro-average, the more accurate we calculate the FLR effect. It is known that the FLR effect plays an important role in determining the ITG growth rate especially for higher n modes [11]. Therefore, we expect that with the application of the improved gyro-average method, the correction to the gyro-average procedure can make significant changes for the ITG growth rates, especially for those high n modes.

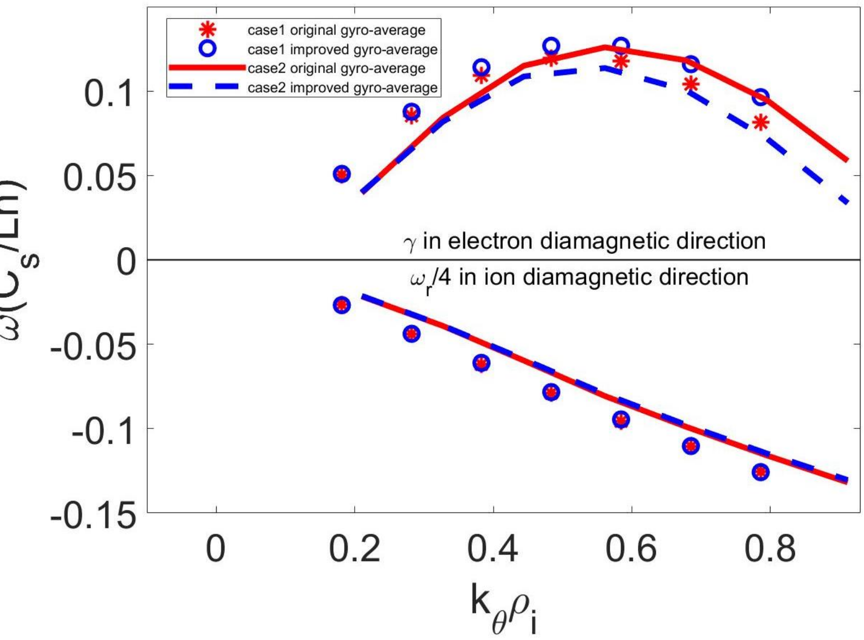

Fig.8 the growth rate and real frequency vs wavenumber in EAST geometry.

The GTC linear ITG simulation results are shown in Fig. 8, where the linear growth rate and frequency varies with poloidal wavelength $k_\theta \rho_i$. In this figure, the blue color represents simulation results using improved four-point average method, while the red color represent simulation results using original four-point average method; case 1 and case 2 represent two different radial domains used in the simulation. As is discovered in Section 2, the coordinate non-orthogonality varies in the poloidal plane. In order to demonstrate its consequence on the linear instability, we artificially set the radial simulation domain: $r \subset [0.55a, 0.95a]$ for case 1, and $r \subset [0.30a, 0.70a]$ for case 2.

As can be seen in Fig. 8, for either case 1 or case 2, the linear growth rate using the improved four-point average converges to that using the original four-point average in the long wavelength limit. With the poloidal/toroidal wavenumber increasing, the FLR effect becomes more important, and the difference for linear growth rate between the two gyro-average methods becomes larger. This trend is demonstrated in Fig. 8 as well. The difference for real frequency is mainly determined by the diamagnetic frequency ω_*, which has little to do with the FLR effect and thus is the real frequency indistinguishable between different gyro-average methods. However, the real frequency for case 1 (outer radial domain) is generally larger than that for case 2 (inner radial domain). This is due to the fact that the average magnetic field for case 1 is smaller than that for case 2 and thus the corresponding diamagnetic frequency is larger for case 1 when the most unstable outside middle plane is considered.

6. Conclusion

In this paper, we have found the main source of inaccuracy introduced by the original gyrophase-average procedure in a realistic tokamak geometry, i.e., the non-orthogonality of the Boozer coordinates [3,10], and developed an innovative multi-point average method to improve the computing accuracy. The effectiveness and accuracy of this new method is demonstrated by a number of benchmark cases such as consistency check and solving gyrokinetic Poisson equation. For the conventional ITG instability case, we find that the improved four-point average method calculates the FLR effect more accurately, demonstrated by the difference of the linear growth rates in the short wavelength range between this new four-point average method and the original one. Based on the improved multi-point average method, we plan to simulate turbulence physics in the edge of tokamak, where this new method can find broader applications for its usefulness.

Acknowledgement:

This work is supported by National MCF Energy R & D Program of China Nos. 2019YFE03060000 and 2015GB110000, and by NSFC under Grant No. 11975201.

References:

[1] W.W. Lee, J. Comput. Phys. 72 (1987) 243.
[2] W.W. Lee, Phys. Fluids 26 (1983) 556.
[3] Z. Lin, W.W. Lee, Phys. Rev. E 52 (1995) 5646.
[4] D.H.E. Dubin, J.A. Krommes, C. Oberman, W.W. Lee, Phys Fluids 26 (1983) 3524.
[5] W.D. D'Haeseleer, W.N. Hitchon, J.D. Callen Flux Coordinates and Magnetic Field Structure Springer (1991)
[6] R. B. White. The Theory of Toroidally Confined Plasmas[M]. World Scientific Imperial College Press,2006. Revised second edition 2006.
[7] A.M. Dimits, G. Bateman, M.A. Beer, et al., Phys. Plasmas 7 (2000) 969.
[8] Z. Lin, T. S. Hahm, W. W. Lee, W. M. Tang, and R. White, Science 281, 1835 (1998).
[9] M. J. LeBrun and T. Tajima, Bull. Am. Phys. Soc. 39,1533 (1994).

[10] Yong Xiao, Ihor Holod, Zhixuan Wang, Zhihong Lin, and Taige Zhang. Physics of Plasmas 22, 022516 (2015);
[11] Akira Hirose. Physics Review Letters55, 5(1985).
[12] P. J. Catto. Generalized Gyrokinetics[J].1981 Plasma Physics 23 639
[13] Frieman E. A., Chen L. Phys. Fluids, 1982. (25):502.
[14] T.S. Hahm. The Physics of Fluids 31, 2670 (1988)
[15] W. X. Wang, Z. Lin, W. M. Tang, W. W. Lee, S. Ethier, J. L. V. Lewandowski, G. Rewoldt, T. S. Hahm, and J. Manickam. Phys. Plasmas 13, 092505 (2006)
[16] Lei Qi, Jaemin Kwon, T.S. Hahm, and Gahyung Jo. Phys. Plasmas 23, 062513 (2016)